MEDTVT-R1: A MULTIMODAL LLM EMPOWERING MEDICAL REASONING AND DIAGNOSIS

Anonymous authors
Paper under double-blind review

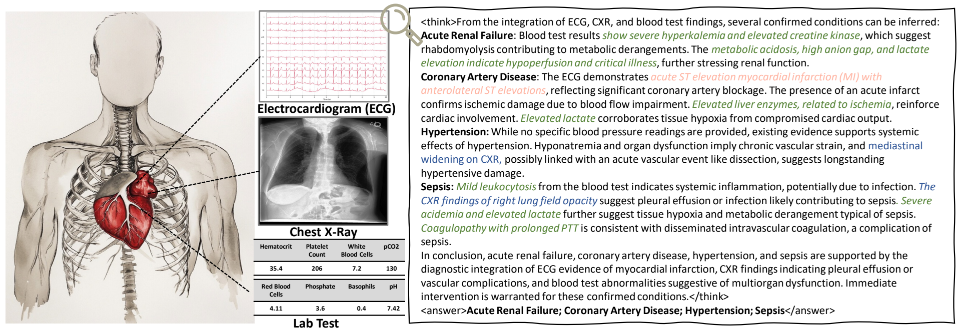

Figure 1: Overview of **MedTVT-R1**: MedTVT-R1 seamlessly integrates Electrocardiogram (**T**ime Series), Chest X-ray (**V**isual Image), and Blood Test (**T**abular Data) to deliver comprehensive long-text **Med**ical reasoning and diagnosis across various diseases.

ABSTRACT

Accurate and interpretable multi-disease diagnosis remains a critical challenge in medical research, particularly when leveraging heterogeneous multimodal medical data. Current approaches often rely on single-modal data, limiting their ability to comprehensively understand complex diseases. To address this, we propose MedTVT-R1, a novel Multimodal Large Language Model (MLLM) framework designed to integrate clinical multimodal data for reasoning and diagnosing multiple diseases. We construct MedTVT-QA, a curated instruction dataset that provides question-answer pairs for physiological-level interpretations and disease-level diagnoses with a Chain of Evidence approach. MedTVT-R1 incorporates a modality perception layer to capture inter-modal dependencies and adaptively weight modality contributions. Additionally, we employ Group Relative Policy Optimization (GRPO)-based Reinforcement Fine-Tuning with a Jaccard Reward function to enhance diagnostic reasoning. Experimental results demonstrate MedTVT-R1's superiority in multimodal feature utilization and multi-disease diagnosis, offering significant potential for clinical applications such as diagnostic report generation and comorbidity reasoning. The dataset and code will be available on GitHub.

1 INTRODUCTION

The rapid development of artificial intelligence (AI) has profoundly reshaped the landscape of medical research and clinical practice, especially in demonstrating significant progress and potential in medical data analysis (Çallı et al., 2021; Liu et al., 2021; Hernandez et al., 2022; Sumon et al., 2025) and disease diagnosis (Cassar et al., 2009; Ghaffar Nia et al., 2023), with an extensive impact (Elstein, 2004).

At present, most existing studies primarily rely on single-modal medical data to perform disease diagnosis (Chen et al., 2024b; Hernandez et al., 2022; Yao et al., 2024; Ansari et al., 2023). Although these single-modal approaches demonstrate certain effectiveness within their respective specific domains, their perception of physiology is often too limited to offer a holistic and comprehensive understanding of complex diseases. Taking diabetes as an example, its physiological manifestations are typically reflected across multiple modalities, such as altered heart rate variability in electrocardiograms (ECG), pulmonary complications observable in chest X-rays (CXR), and abnormal glucose or lipid levels revealed by laboratory blood tests (LAB) (Lin et al., 2021). Therefore, to address the risk of incomplete or inaccurate diagnoses resulting from reliance on a single modality, it is essential to integrate multimodal medical data for comprehensive and in-depth analysis of complex diseases (Alcaraz & Strodthoff, 2024; Steyaert et al., 2023).

Consequently, there are a number of efforts that have emerged to explore leveraging multimodal medical data for disease diagnosis (Kline et al., 2022; Steyaert et al., 2023; Venugopalan et al., 2021; Abdelaziz et al., 2021). Nevertheless, these methods often make only simple and direct determinations about the presence or absence of a specific disease (Gundapaneni et al., 2024; Kumar, 2022), but struggle with performing robust long-text diagnostic reasoning and generating interpretable clinical insights for multiple diseases, which severely hinders their practical application.

Recently, multimodal large language models (MLLMs) (Zhang et al., 2023; Li et al., 2023a; Liu et al., 2023; 2024c; Tian et al., 2025; Wu et al., 2024) have undergone rapid development and achieved impressive results in a variety of tasks, such as vision-language and audio-language tasks. They have demonstrated strong capabilities in integrating, generalizing, and reasoning across diverse data modalities, offering promising potential for generating interpretable disease diagnosis reports from medical data. Although several pioneering studies have made preliminary attempts to apply MLLMs in the medical field, such as for ECG analysis (Zhao et al., 2024; Tian et al., 2024) or medical image reporting (Shentu & Al Moubayed, 2024; Liu et al., 2024a; Tanno et al., 2025) tasks, these works are still limited to single modalities (*e.g.*, ECG, CXR) and remain at physiological-level understanding rather than disease-level reasoning. Therefore, an MLLM that can perceive and integrate heterogeneous multimodal medical data, thereby enabling interpretable multi-disease reasoning and diagnosis, remains a significant gap in current research.

From above observations, we propose **MedTVT-R1**—an MLLM leveraging clinical multimodal data's complementarity/corroboration for multi-disease reasoning/diagnosis (advances in Figure 1). To this end, we construct **MedTVT-QA**—the first instruction dataset covering three modalities (ECG, CXR, LAB) with QA pairs. It includes physiological interpretations and disease-level diagnoses via a Chain of Evidence (CoE) (using cross-modal complementarity/corroboration), laying a foundation for MLLMs' progressive multimodal integration for physiological perception/multi-disease diagnosis. We also add a Modality Perception Layer (MPL) to MedTVT-R1, capturing cross-modal dependencies and adaptively weighting modality contributions by disease relevance to maximize cross-modal interaction/information use. Inspired by DeepSeek-R1 (Guo et al., 2025), we adopt Reinforcement Fine-Tuning (RFT) via Group Relative Policy Optimization (GRPO) for post-training, with a Jaccard Reward function for multi-disease scenarios—boosting reasoning capability. Extensive experiments show MedTVT-R1's superiority in single-modality physiological understanding and multimodal disease diagnosis, with implications for clinical MLLM applications (e.g., interpretable diagnostic reports, complex comorbidity reasoning). Our contributions are summarized as follows:

- We introduce MedTVT-QA, the first medical instruction dataset that features heterogeneous modalities including ECG (Time Series), CXR (Visual Images), and LAB (Tabular Data).
- We propose MedTVT-R1, a novel MLLM framework that fully leverages the complementarity and mutual corroboration among clinical multimodal data for interpretable diagnosis of complex comorbidities.
- We employ a Reinforcement Fine-Tuning (RFT) strategy based on Group Relative Policy Optimization (GRPO) incorporating a dedicated Jaccard reward function to unlock data potential and enhance the model's reasoning accuracy.
- Extensive experiments demonstrate that MedTVT-R1 achieves state-of-the-art performance in physiological representation understanding across various modalities and multimodal diagnosis and report generation for comorbidity.

2 Related Work

MLLM for Medical Diagnosis. The application of Multimodal Large Language Models (MLLMs) in medical diagnosis has gained significant attention due to their ability to process and integrate diverse data modalities, such as text (Li et al., 2025; Liévin et al., 2024; Jin et al., 2024; Gallifant et al., 2025), images (Irvin et al., 2019; Lee et al., 2025; 2023; Lu et al., 2024b), and tabular data (Bisercic et al., 2023; Huang et al., 2024). Early works focused on single-modal approaches, such as text-based models for clinical note analysis (Jin et al., 2024; Yuan et al., 2024; Liévin et al., 2024), image-based models for radiology interpretation (Lee et al., 2025; Irvin et al., 2019), or ECG-based models for cardiac status analysis (Zhao et al., 2024; Yu et al., 2023; Lan et al., 2025; Yang et al., 2025). Although significant advancements have been made, existing research has yet to integrate **T**ime series data (e.g., Electrocardiograms), **V**isual data (e.g., chest X-rays), and **T**abular data (e.g., lab results) into a unified framework for comprehensive **Med**ical disease analysis and diagnosis. To bridge this gap, we introduce **MedTVT-R1**, a multimodal large language model designed to seamlessly combine CXR, ECG, and lab data through cross-modal interactions and contribution-aware operator, enabling accurate and interpretable disease diagnosis.

Reinforcement Learning with Verifiable Rewards. Group Relative Policy Optimization (GRPO) (Guo et al., 2025), unlike Proximal Policy Optimization (PPO) (Yu et al., 2022; Schulman et al., 2017) which estimates advantages through a reward model, approximates advantages by obtaining multiple samples from the LLM using the same prompt, with the advantage being the normalized reward for each response within its set of generated responses, achieving notable success in text-based tasks (Shao et al., 2024; Ramesh et al., 2024; Dao & Vu, 2025) such as summarization and dialogue generation, as well as vision tasks (Liu et al., 2025; Tan et al., 2025) like image captioning. Recently, GRPO has been applied to medical image analysis (Lai et al., 2025; Pan et al., 2025). However, it has not yet been utilized for multimodal tasks in the crucial area of multi-disease diagnosis, which requires the integration of text, images, time series, and tabular data. In this work, we are pioneering the application of GRPO with a newly designed reward function, the Jaccard Reward, to enhance the accuracy of multi-disease prediction.

3 Methodology

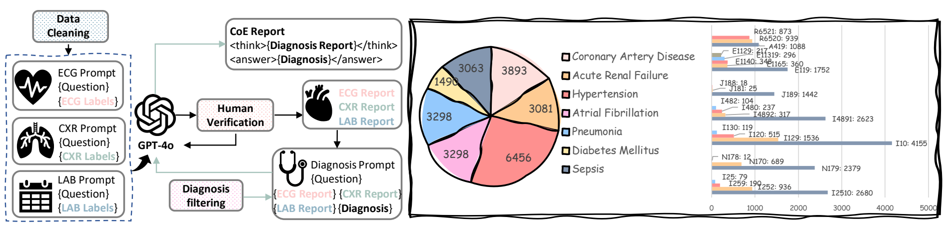

(a) Pipeline of Dataset Construction (b) Disease Distribution of Training Data

Figure 2: MedTVT-QA dataset construction and disease distribution. (a) Pipeline of Dataset Construction: labels are refined to ensure consistency, prompts guide GPT-4o in generating verified physiological-level reports, which are combined with diagnostic labels to produce disease-level reports. Diagnostic labels are organized into seven primary categories with detailed subtypes. (b) Disease distribution of MedTVT-QA, with subtypes classified by ICD-10 codes. More details can be found in Appendix B.

3.1 MedTVT-QA

To enable MLLMs to perform physiological understanding and disease diagnosis from heterogeneous multimodal medical data, we curate patient-level ECG readings, blood test results, and chest X-ray (CXR) images from the MIMIC-IV family of datasets (Johnson et al., 2020; Gow et al., 2023; Johnson et al., 2019), facilitated by Symile (Saporta et al., 2024). All modalities are acquired from the same individuals within a clinically proximate period during hospitalization, yielding 8,706 aligned multimodal combinations (8,331 for training, 375 for testing). Additional diagnostic labels are sourced from MIMIC-IV-ECG-EXT-ICD (Strodthoff et al., 2024). These data underpin the construction of multimodal question–answer (QA) pairs for both physiological representation analysis and disease-level diagnostic reasoning, as illustrated in Figure 2(a).

QA Pairs on Physiological-level Representation Analysis. To enable MLLMs to acquire a basic comprehension of the physiological meanings represented by each modality, *i.e.*, ECG, CXR, and LAB, and to lay the groundwork for subsequent multi-disease reasoning and diagnosis based on multimodal data, we first construct QA pairs focused on physiological-level analysis for each modality. Specifically, taking the ECG modality as an example, we design a rigorous prompt with reference to physiological-level annotations, which consists of Role Setting, Task Description, Answer Guidance, and Answer Format to instruct GPT-4o (Achiam et al., 2023), as outlined below:

Role Setting: You are a renowned cardiologist with expertise in interpreting electrocardiograms (ECGs).
Task Description: The ECG analysis has yielded the following labels: {`labels`}. Based on these labels, please address the question: {`question`}.
Answer Guidance: Your response should incorporate all relevant labels, excluding any unrelated ones. Provide a synthesis of the labels, focusing on clinical significance.
Answer Format: Begin with a brief introduction to your analysis. Provide detailed explanations for each specific ECG label. Offer a concise summary.

Here, {`labels`} refers to physiological-level annotations for the ECG data, such as Sinus Rhythm or Left Bundle Branch Block. {`question`} is randomly sampled from several carefully crafted question templates, such as 'What information can be derived from the ECG?'. An example of a constructed QA pair that summarizes and analyzes the physiological representations encompassed in ECG is:

> ***Question*:** What information can be derived from the ECG ¡ecg¿?
> ***Answer*:** ECG Analysis: Upon evaluating the electrocardiogram (ECG), the following observations can be made:
> 1. Sinus Rhythm: The heart is under the control of the sinoatrial (SA) node, which is the natural pacemaker. This finding suggests that the electrical activity of the heart is originating from the SA node and progressing through the normal conduction pathway, leading to a regular rhythm. This is a foundational indicator of organized cardiac activity.
> 2. Left Bundle Branch Block (LBBB): There is evidence of delayed or disrupted conduction through the left bundle of the heart's electrical conduction system. This results in a characteristic pattern on the ECG, with a widened QRS complex (¿120 ms) and specific morphologies in leads, such as a broad, notched appearance in V5-V6 and an absence of normal septal depolarization. LBBB may occur in conditions like ischemic heart disease, cardiomyopathy, or hypertension-induced structural changes, though it can also occasionally be found in asymptomatic individuals.
> Summary: The heart demonstrates a sinus rhythm, indicating normal initiation of electrical activity. However, the presence of a left bundle branch block signifies an abnormality in electrical conduction, often associated with underlying cardiac pathology. As a whole, this ECG is classified as abnormal due to the conduction disturbance, warranting further investigation to assess structural or functional cardiac issues.

Similar prompts are also applied to CXR and LAB data to organize the corresponding physiological-level QA pairs for each modality. It is worth noting that, for LAB data, we group 50 common laboratory indicators into seven categories according to their physiological significance to facilitate processing. The content generated above for physiological-level representation analysis undergoes manual review and revision by professionals to ensure its rationality and reliability. More details on physiological-level annotation and examples of QA pairs for each modality can be found in the Appendix A to C.

QA Pairs on Disease-level Diagnostic Reasoning. Building upon the aforementioned completed physiological-level representation analysis for each modality, we further construct QA pairs that fully integrate information across modalities and conduct disease-level diagnostic reasoning, thereby enhancing the capability of MLLMs to handle complex multiple diseases. We focus on seven common and clinically significant diseases for which supporting evidence can be found in ECG, CXR, and LAB data, including *Coronary Artery Disease, Acute Renal Failure, Hypertension, Atrial Fibrillation, Pneumonia, Diabetes Mellitus,* and *Sepsis*, each of which contains several subtypes, with details in the Appendix B. The corresponding statistics are presented in Figure 2 (b). We also employ a four-element prompt with reference to disease-level annotations to instruct GPT-4o, and compel its response to include a Chain of Evidence (CoE) to fully leverage the complementarity and mutual corroboration among modalities, thereby thoroughly extracting multimodal evidence for disease diagnosis, as follows:

> ***Role Setting*:** You are a renowned diagnostician with expertise in integrating ECG, CXR, and blood test results.
> ***Task Description*:** The following diagnostics have been provided:
> • ECG Analysis: {`ecg_report`}
> • CXR Analysis: {`cxr_report`}
> • Blood Test Analysis: {`blood_test_report`}
> • Diseases: {`result_diseases`}
> You need to pretend that the ECG, CXR, and blood test analyses are based on your interpretation of the raw data, and the final diagnosis is your synthesis of these three diagnostic methods, please address the question: {`question`}
> ***Answer Guidance*:** Please find definitive evidence from the ECG, CXR, and blood test results, leveraging the complementarity and mutual corroboration of these three modalities, to robustly prove the reasons why the patient has the diseases I provided. Your response must include every disease I provided, using the exact wording I provided, and you must not mention any diseases other than those I provided. Please make sure to provide evidence for these diagnoses! These are confirmed conditions.
> ***Answer Format*:** <think>{Diagnostic evidence synthesized from the three modalities}</think>\n <answer>{disease1; disease2; ...}</answer>

Here, {`ecg_report`}, {`cxr_report`}, and {`blood_test_report`} respectively represent the physiological-level analyses of the three modalities. {`result_diseases`} refers to the disease-level annotation of the sample. {`question`} is randomly sampled from several carefully crafted question templates, such as 'Can you analyze my ECG, CXR and lab result to determine my probable conditions?'. The CoE is implemented by 'Please find definitive evidence...'. The content obtained in this process is also reviewed by professionals to enhance its trustworthiness. An example of a QA pair that integrates multimodal information to mine evidence for multi-disease reasoning and diagnosis is shown in Figure 3, and the complete version is provided in the Appendix E.

3.2 MedTVT-R1

Based on the meticulously constructed MedTVT-QA dataset described above, we propose MedTVT-R1, an MLLM framework capable of fully exploiting the complementarity and mutual corroboration of multimodal medical data for interpretable multi-disease reasoning and clinical diagnosis. In the following, we will introduce the model architecture and training strategy of MedTVT-R1 in detail.

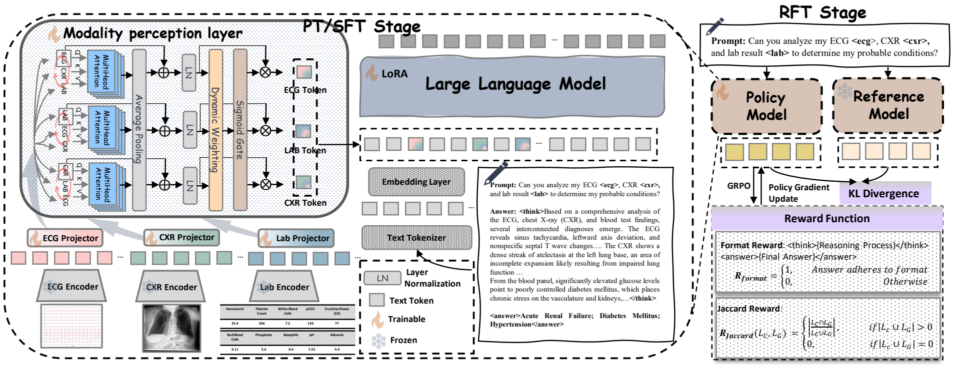

Figure 3: Pipeline of MedTVT-R1. Pretraining processes ECG, CXR, and LAB data through encoders and projectors, combined with prompts, to train projectors and LLM's LoRA for enhanced physiological understanding. The SFT stage adds a Modality Perception Layer for interaction and integration, refining disease analysis. The RFT stage applies GRPO, using the SFT-trained model for policy and inference, optimizing KL divergence and reward loss.

3.2.1 ARCHITECTURE

The proposed MedTVT-R1 mainly consists of modality-specific encoders and projectors, a Modality Perception Layer (MPL), and a Large Language Model (LLM), with its overall architecture illustrated on the left side of Figure 3. Given the raw data of ECG signals $\mathbf{X_E} \in \mathbb{R}^{N \times L}$, CXR images $\mathbf{X_C} \in \mathbb{R}^{C \times H \times W}$, and LAB tables $\mathbf{X_L} \in \mathbb{R}^{N'}$, they are first processed by their respective modality-specific encoders for feature extraction, and then the encoded features are fed into modality-specific projectors to a shared dimension d for alignment and compatibility with the textual embedding space of the LLM, facilitating seamless integration between multimodal features and textual tokens; this process can be formulated as follows:

$$\mathbf{Z_E} = g_{\mathrm{E}}(f_{\mathrm{E}}(\mathbf{X_E})) \in \mathbb{R}^d, \quad \mathbf{Z_C} = g_{\mathrm{C}}(f_{\mathrm{C}}(\mathbf{X_C})) \in \mathbb{R}^d, \quad \mathbf{Z_L} = g_{\mathrm{L}}(f_{\mathrm{L}}(\mathbf{X_L})) \in \mathbb{R}^d, \tag{1}$$

where $\mathbf{Z_{E/C/L}}$ denotes the projected multimodal features, and $f_{\mathrm{E/C/L}}$ and $g_{\mathrm{E/C/L}}$ represent the modality-specific encoders and projectors, respectively.

Subsequently, to enable efficient interaction and fusion among modalities, we introduce a Modality Perception Layer (MPL), which comprises a Cyclic Multi-Head Attention (CMHA) mechanism and a Contribution-Aware Operator (CAO). Specifically, the projected features $\mathbf{Z_E}$, $\mathbf{Z_C}$, and $\mathbf{Z_L}$ are first processed by the CMHA mechanism, in which each modality feature cyclically serves as the Query, Key, and Value to compute multi-head attention, enabling comprehensive capture of cross-modal dependencies and facilitating in-depth information exchange among ECG, CXR, and LAB features. After one round of cycling, the outputs are fused through average pooling, while a residual connection is employed to preserve modality-specific information. This process can be formulated as follows:

$$\mathbf{F} = \text{AveragePooling}(\text{CMHA}(\mathbf{Z_E}, \mathbf{Z_C}, \mathbf{Z_L})), \quad \mathrm{M}_{\mathbf{E/C/L}} = \mathbf{Z_{E/C/L}} + \mathbf{F}, \tag{2}$$

where $\mathrm{M}_{\mathbf{E/C/L}}$ denotes the updated features of each modality, which encapsulate both modality-specific and modality-shared information. Recognizing that each modality contributes in varying degrees to the reasoning and diagnosis of various diseases, for example, ECG features are relatively more important for detecting Coronary Artery Disease, we design a Contribution-Aware Operator that adaptively assigns weights to the features of each modality based on the diagnostic context, which can be formulated as follows:

$$\mathbf{T_E}, \mathbf{T_C}, \mathbf{T_L} = \sigma(h[\mathbf{M_E} : \mathbf{M_C} : \mathbf{M_L}]) \otimes (\mathbf{M_E}, \mathbf{M_C}, \mathbf{M_L}), \tag{3}$$

where $[:]$ denotes the concatenation operation, h is a learnable transformation matrix, σ represents the Sigmoid activation, and $\otimes$ denotes element-wise multiplication. The final multimodal features $\mathbf{T_E}$, $\mathbf{T_C}$, and $\mathbf{T_L}$ are used to replace the placeholders `<ecg>`, `<cxr>`, and `<lab>` in the text tokens, which are obtained by processing the input prompt through the tokenizer and embedding layer. An example input prompt could be: 'What illnesses might be indicated by the findings from my ECG <ecg>, CXR <cxr>, and blood work <lab>?'. The resulting sequence $\mathbf{T}_{\text{input}} = \{\mathbf{T}_{\mathrm{Q}}, \mathbf{T}_{\mathrm{E}}, \mathbf{T}_{\mathrm{C}}, \mathbf{T}_{\mathrm{L}}, \mathbf{T}_{\mathrm{A}}\}$ is then fed into the LLM, where $\mathbf{T}_{\mathrm{Q}}$ and $\mathbf{T}_{\mathrm{A}}$ are derived from the QA pairs in the MedTVT-QA dataset.

3.2.2 Training Strategy

We employ a three-stage training strategy for MedTVT-R1, which includes Pre-training (PT), Supervised Fine-Tuning (SFT), and Reinforcement Fine-Tuning (RFT), to progressively enhance its ability to perceive the physiological representations of each modality and integrate multimodal information for interpretable multi-disease reasoning and diagnosis.

Pre-training. With the aim of helping the model form an initial understanding and awareness of the physiological significance across all modalities, we first perform pre-training using physiological-level QA pairs from the MedTVT-QA dataset. During this stage, the projectors and the Low-Rank Adaptation (LoRA) modules embedded in the LLM are set as trainable, while the other components remain frozen. Notably, the MPL module is absent at this stage as no cross-modal interaction is involved. The optimization objective is to maximize the likelihood of generating the target response tokens, formalized as:

$$\mathcal{L}_{\text{PT}} = -\mathbb{E}_{(\mathbf{T_Q}, \mathbf{T_{E/C/L}}, \mathbf{T_A}) \sim \mathcal{D}} \sum_{t=1}^{T} \log \pi_\theta(y_t \mid \mathbf{T_Q}, \mathbf{T_{E/C/L}}, y_{<t}), \tag{4}$$

where $\pi_\theta(y_t \mid \cdot)$ denotes the conditional probability of generating the t-th token y_t, given the prompt, modality features, and the previously generated tokens $y_{<t}$.

Supervised Fine-Tuning. With the pretrained model that already demonstrates a solid understanding of the physiological significance of each modality, we further conduct SFT based on disease-level QA pairs with CoE logic from the MedTVT-QA dataset to equip the model with the capability to synthesize multimodal representations and uncover the complementarity and mutual corroboration among modalities for multi-disease reasoning and diagnosis. During this stage, the MPL and the LoRA modules embedded in the LLM are set to be trainable while the other components remain frozen, and the optimization objective is similar to that of the pre-training stage, namely:

$$\mathcal{L}_{\text{SFT}} = -\mathbb{E}_{(\mathbf{T_Q}, \mathbf{T_E}, \mathbf{T_C}, \mathbf{T_L}, \mathbf{T_A}) \sim \mathcal{D}} \sum_{t=1}^{T} \log \pi_\theta(y_t \mid \mathbf{T_Q}, \mathbf{T_E}, \mathbf{T_C}, \mathbf{T_L}, y_{<t}). \tag{5}$$

Reinforcement Fine-Tuning. To unlock the potential of the constructed dataset and boost the model's reasoning performance, inspired by the advancements of DeepSeek-R1, we perform RFT using Group Relative Policy Optimization (GRPO) under the Reinforcement Learning with Verifiable Rewards (RLVR) framework. The training corpus and trainable components remain consistent with those in the SFT stage. The optimization objective can be formulated as:

$$\max_{\pi_\theta} \mathbb{E}_{\mathbf{A} \sim \pi_\theta(\mathbf{Q})} \left[R_{\text{RLVR}}(\mathbf{Q}, \mathbf{A}) \right] = \left[R(\mathbf{Q}, \mathbf{A}) - \beta \text{KL} \left[\pi_\theta(\mathbf{A} \mid \mathbf{Q}) \,\|\, \pi_{\text{ref}}(\mathbf{A} \mid \mathbf{Q}) \right] \right], \tag{6}$$

where π_θ and π_{ref} are the policy model and the reference model, respectively. R is the verifiable reward function. KL $[\pi_\theta(\mathbf{A} \mid \mathbf{Q}) \,\|\, \pi_{\text{ref}}(\mathbf{A} \mid \mathbf{Q})]$ penalizes divergence from the reference policy π_{ref}, ensuring both correctness and alignment with prior knowledge. The hyperparameter β controls the trade-off between reward maximization and policy regularization.

GRPO directly compares the relative quality of responses within a group without requiring an additional critic model. Specifically, given a question $\mathbf{Q}$, GRPO first generates G candidate responses $\{o_1, o_2, \ldots, o_G\}$ according to the current policy $\pi_{\theta_{\text{old}}}$, which are then assigned rewards $\{r_1, r_2, \ldots, r_G\}$. The relative quality of these responses is calculated by normalizing the rewards using their mean and standard deviation. GRPO encourages the model to prioritize responses with higher relative rewards, fostering improved performance without requiring a separate critic.

The verifiable reward function R consists of the Format Reward and the Jaccard Reward, *i.e.*, $R = R_{\text{F}} + R_{\text{J}}$, ensuring both prediction accuracy and structural consistency. In line with DeepSeek-R1, the Format Reward R_{F} is used to enforce the model's compliance with predefined formatting rules for the <think> and <answer> tags. The Jaccard Reward R_J is a novel, meticulously designed reward function tailored for multi-disease diagnosis, which evaluates the alignment between the model's predictions and the ground truth by leveraging the Jaccard similarity coefficient, thereby quantifying the overlap between the predicted and actual disease sets. Specifically, for each model completion and its corresponding ground truth, the disease sets within the <answer> tags are first extracted using regular expressions and denoted as $L_C = \{l_{c_1}, l_{c_2}, \ldots, l_{c_m}\}$ and $L_G = \{l_{g_1}, l_{g_2}, \ldots, l_{g_n}\}$,

Method	LLM	NLG				CE			
		BLEU	METEOR	ROUGE	BERT	PRECISION	RECALL	F1 SCORE	AUC
General-purpose MLLMs									
InternVL3-1B (Zhu et al., 2025)	InternVL3-1B	0.0178	0.1884	0.1265	0.8188	0.3333	0.1333	0.1904	0.5053
LLaVA-1.5-7B (Liu et al., 2024b)	Vicuna-7B	0.0029	0.0809	0.0681	0.7796	0.2495	0.1279	0.1691	0.5004
LLaVA-One-Vision-7B (Li et al., 2024b)	Qwen2-7B	0.0144	0.1618	0.1168	0.8016	0.3120	0.1247	0.1782	0.4975
Qwen2.5-VL-3B-Instruct (Bai et al., 2025)	Qwen2.5-3B-Instruct	0.0218	0.2031	0.1331	0.8181	0.3493	0.1397	0.1995	0.5000
Mini-InternVL-Chat-2B-V1-5 (Bai et al., 2025)	InternLM2-Chat-1.8B	0.0092	0.1347	0.0959	0.8008	0.2176	0.1343	0.1661	0.5015
Molmo-7B-O-0924 (Deitke et al., 2024)	OLMo-7B	0.0155	0.1456	0.1070	0.8028	0.0295	0.0608	0.0398	0.5001
Deepseek-VL-1.3B-Chat (Lu et al., 2024a)	Deepseek-1.3B-Chat	0.0341	0.1756	0.1435	0.8128	0.2510	0.1278	0.1694	0.5021
LLaVA-NeXT-8B (Li et al., 2024a)	LLaMA3-8B	0.0145	0.1532	0.1067	0.8145	0.2674	0.1294	0.1744	0.4987
Medical domain-specific MLLMs									
Med-Flamingo (Moor et al., 2023)	LLaMA2-7B	0.0567	0.2134	0.1568	0.8328	0.3255	0.1427	0.1984	0.5201
LLaVA-Med (Li et al., 2023b)	LLaVA-7B	0.0735	0.2358	0.1637	0.8321	0.3028	0.1578	0.2075	0.5318
HuatuoGPT-Vision (Chen et al., 2024a)	LLaVA-v1.6-34B	0.0624	0.2017	0.1389	0.8048	0.2867	0.1622	0.2072	0.5038
MedTVT-R1 w/o PT	LLaMA3.2-1B	0.1131	0.3280	0.2043	0.8599	0.4980	0.5208	0.4672	0.5851
MedTVT-R1 w/o RFT	LLaMA3.2-1B	0.1325	0.3499	0.2261	0.8660	0.5237	0.5783	0.4992	0.6242
MedTVT-R1	LLaMA3.2-1B	**0.1353**	**0.3536**	**0.2295**	**0.8652**	**0.5407**	**0.5908**	**0.5190**	**0.6554**

Table 1: Comparison of MedTVT-R1 with various MLLMs and its variants on disease-level reasoning and diagnostic capabilities. The table is divided into general-purpose MLLMs and medical domain-specific MLLMs. The proposed MedTVT-R1 highlighted in gray.

where l_{c_i} and l_{g_j} represent individual diseases in the predicted and ground truth sets, respectively. The Jaccard Reward R_J is then computed as:

$$R_J(L_C, L_G) = \begin{cases} \frac{|L_C \cap L_G|}{|L_C \cup L_G|}, & \text{if } |L_C \cup L_G| > 0, \\ 0, & \text{if } |L_C \cup L_G| = 0. \end{cases} \tag{7}$$

When the union of the sets is not empty, the R_J is determined by the ratio of the intersection size to the union size, thereby capturing the degree of overlap between the prediction and ground truth. If the union is empty, the R_J is set to zero to ensure robustness against invalid or incomplete outputs. Therefore, the Jaccard reward encourages the model to generate outputs that are highly consistent with the ground truth labels, which effectively helps improve both the accuracy and reliability in multi-disease diagnosis scenarios.

4 Experiments

4.1 Training Details and Metrics

Training Details. We conduct all experiments on a server equipped with eight NVIDIA A800 80GB GPUs. For the LLM, we choose LLaMA 3.2-1B (Grattafiori et al., 2024) and integrate the LoRA modules (Hu et al., 2022) with a rank of 8 for fine-tuning. For the modality-specific encoders, we use the pre-trained weights from ECGFM-KED (Tian et al., 2024), ViT-B/16 (Dosovitskiy et al., 2020), and Symile (Saporta et al., 2024) for ECG, CXR, and LAB, respectively. All modality-specific projectors adopt the Dense block architecture from MuMu-LLaMA (Liu et al., 2024c), with the embedding dimension d set to 2048. During training, the PT and SFT stages are each trained for 20 epochs, while the RFT stage is trained for 500 iterations using the open-source Trainer framework, with G in GRPO set to 8. **Metrics.** The effectiveness of multi-disease reasoning and diagnosis was evaluated from two perspectives. First, the descriptive accuracy of the generated diagnostic text was assessed using natural language generation (NLG) metrics, including BLEU, METEOR, ROUGE, and BERTScore. Second, the classification accuracy of multi-label disease categories in the responses was evaluated using clinical efficacy (CE) metrics, such as PRECISION, RECALL, F1 SCORE, and AUC.

4.2 Quantitative Analysis

Disease-level Diagnostic Reasoning Results. Since no existing multimodal large model can jointly process ECG signals, medical images, and tabular data, we convert ECG signals into images and LAB data into text for a fair comparison. Table 1 reports results for our MedTVT-R1 against two categories of state-of-the-art MLLMs: *(i) General-purpose* — InternVL3-1B (Zhu et al., 2025), LLaVA-1.5-7B (Liu et al., 2024b), LLaVA-One-Vision-7B (Li et al., 2024b), Qwen2.5-VL-3B-Instruct (Bai et al., 2025), Mini-InternVL-Chat-2B-V1-5 (Bai et al., 2025), Molmo-7B-O-0924 (Deitke et al., 2024), Deepseek-VL-1.3B-Chat (Lu et al., 2024a), and LLaVA-NeXT-8B (Li et al., 2024a); *(ii) Medical-specific* — Med-Flamingo (Moor et al., 2023), LLaVA-Med (Li et al., 2023b), and HuatuoGPT-Vision (Chen et al., 2024a). These models span 1B–8B parameters and various backbones (InternVL, Vicuna, Qwen, OLMo, Deepseek, LLaMA3), with some incorporating RL or domain-specific pre-training. All inference results were obtained using ModelScope SWIFT (Zhao et al., 2025).

Method	ECG-QA				CXR-QA				LAB-QA			
	BLEU	METEOR	ROUGE	BERT	BLEU	METEOR	ROUGE	BERT	BLEU	METEOR	ROUGE	BERT
General-purpose MLLMs												
InternVL3-1B (Zhu et al., 2025)	0.0186	0.1795	0.1379	0.8282	0.0239	0.1827	0.1273	0.8309	0.0083	0.1234	0.0750	0.7750
LLaVA-1.5-7B (Liu et al., 2024b)	0.0055	0.1084	0.0866	0.8100	0.0034	0.0967	0.0812	0.8012	0.0170	0.1402	0.1133	0.7937
LLaVA-One-Vision-7B (Li et al., 2024b)	0.0313	0.2263	0.1545	0.8322	0.0260	0.1877	0.1325	0.8214	0.0088	0.1362	0.0967	0.7883
Qwen2.5-VL-3B-Instruct (Bai et al., 2025)	0.0304	0.2483	0.1687	0.8418	0.0310	0.1798	0.1261	0.8230	0.0081	0.1129	0.0764	0.7832
Mini-InternVL-Chat-2B-V1-5 (Bai et al., 2025)	0.0102	0.1336	0.0984	0.8112	0.0088	0.1082	0.0825	0.8044	0.0085	0.1286	0.1118	0.7781
Molmo-7B-O-0924 (Deitke et al., 2024)	0.0233	0.1949	0.1341	0.8305	0.0211	0.1813	0.1255	0.8231	0.0091	0.1102	0.1120	0.7587
Deepseek-VL-1.3B-Chat (Lu et al., 2024a)	0.0240	0.1708	0.1162	0.8205	0.0298	0.1510	0.1312	0.8215	0.0118	0.0975	0.1184	0.7675
LLaVA-NeXT-8B (Li et al., 2024a)	0.0091	0.1412	0.1064	0.8009	0.0107	0.1305	0.1307	0.8199	0.0102	0.1057	0.1091	0.7623
Medical domain-specific MLLMs												
Med-Flamingo (Moor et al., 2023)	0.0526	0.2016	0.1728	0.8517	0.0527	0.1978	0.1567	0.8326	0.0190	0.1178	0.1236	0.7768
LLaVA-Med (Li et al., 2023b)	0.0728	0.2218	0.1829	0.8328	0.0618	0.2119	0.1418	0.8418	0.0256	0.1327	0.1318	0.7826
HuatuoGPT-Vision (Chen et al., 2024a)	0.0758	0.2518	0.1910	0.8529	0.0719	0.2249	0.1528	0.8518	0.0211	0.1411	0.1419	0.7736
MedTVT-R1	**0.0831**	**0.3044**	**0.2202**	**0.8650**	**0.0931**	**0.3073**	**0.2121**	**0.8673**	**0.1807**	**0.3827**	**0.3081**	**0.8855**

Table 2: Comparison of MedTVT-R1 with various MLLMs on physiological-level understanding and analysis capabilities. The table is divided into general-purpose MLLMs and medical domain-specific MLLMs. The proposed MedTVT-R1 highlighted in gray.

MedTVT-R1 surpasses both general-purpose and medical-specific baselines in natural language generation and clinical evaluation, demonstrating superior descriptive and diagnostic reasoning for multi-disease scenarios. Table 1 also includes ablations: removing physiological-level pre-training or GRPO-based RFT post-training degrades performance, confirming that 1) physiological-level pre-training endows the model with cross-modal physiological representation capabilities, facilitating more effective multimodal integration during SFT; and 2) GRPO-based RFT leverages the available training data to refine and strengthen multi-disease diagnostic reasoning.

Physiological-level Understanding Results. Following the setup in Disease-level Diagnostic Reasoning, we evaluated MedTVT-R1 on single-modality physiological-level understanding against two categories of state-of-the-art MLLMs. Results in Table 2 show MedTVT-R1 outperforms all competitors. Notably, the designed Physiological-level representation analysis is a challenging long-text generation task ($\geq$ 300 words per instance); MedTVT-R1 still delivers outstanding results, highlighting its strength in handling lengthy, detailed outputs. These findings confirm MedTVT-R1's exceptional performance in long-text generation, effective comprehension of cross-modal physiological data, and robustness in both single-modality perception and multimodal reasoning, establishing it as a leading solution for complex medical data analysis.

Synergistic Advantage of Multi-Modal Integration. To quantify the performance gains derived from the joint utilization of ECG, CXR, and laboratory test data in multi-disease diagnosis, we conducted a modality ablation study. The model was evaluated under seven input configurations: (1) all three modalities, (2–4) pairwise modality combinations, and (5–7) single-modality inputs. For absent modalities, the corresponding input tensor was substituted with zero-valued tensors of matching dimensionality to preserve architectural consistency and isolate the impact of modality exclusion. As reported in Table 3, the full tri-modal configuration attained the highest Micro F1 (0.519), Macro F1 (0.457), and Jaccard (0.389) scores. Excluding any modality led to measurable performance degradation, with the most pronounced declines in Macro F1 observed when CXR or laboratory data were omitted—indicating that specific disease categories derive substantial discriminative benefit from particular modalities. Single-modality inputs yielded markedly inferior results, especially in Macro F1, evidencing the complementary representational strengths of ECG, CXR, and laboratory data. Collectively, these findings substantiate that tri-modal fusion confers a synergistic representational advantage, facilitating more balanced and resilient diagnostic performance across heterogeneous disease categories.

Table 3: Performance comparison under different modality combinations. The values in parentheses indicate the relative performance drop (%) compared to the full three-modality setting.

Modalities	**Micro F1**	**Macro F1**	**Jaccard**
Full	0.519	0.457	0.389
NoLab	0.488 (-6.0%)	0.374 (-18.2%)	0.352 (-9.5%)
NoCXR	0.482 (-7.1%)	0.409 (-10.5%)	0.320 (-17.7%)
NoECG	0.484 (-6.7%)	0.415 (-9.2%)	0.322 (-17.2%)
ECGOnly	0.460 (-11.4%)	0.351 (-23.2%)	0.327 (-15.9%)
CXROnly	0.470 (-9.4%)	0.353 (-22.7%)	0.333 (-14.4%)
LabOnly	0.482 (-7.1%)	0.413 (-9.6%)	0.328 (-15.7%)

Effect of MPL Design and Modality Completeness. Table 4 ablation results confirm the effectiveness of Cyclic Multi-Head Attention (CMHA) and Contribution-Aware Operator (CAO) in the Modality Perception Layer (MPL), plus the criticality of full modality integration in pre-training. CMHA/CAO incorporation boosts performance, validating designs for enhanced modality fusion and adaptive modality weighting across diseases. For modality composition, fusing all three modalities (ECG, CXR, LAB) yields the best results; removing any degrades performance, with ECG exclusion causing the sharpest METEOR/ROUGE drops (attributed to strong disease-cardiac activity associations). These findings emphasize that advanced fusion mechanisms and full modality integration are both essential for optimal diagnostic reasoning.

Table 4: The ablation of the Cyclic Multi-Head Attention (CMHA) and Contribution-Aware Operator (CAO) in the Modality Perception Layer (MPL), and the impact of modal missingness during pre-training. Metrics: METEOR, ROUGE, RECALL, F1. Default settings are highlighted.

(a) Ablation study of MPL.

MPL		NLG		CE	
CMHA	CAO	MET.	ROU.	REC.	F1
✗	✓	0.3455	0.2013	0.5733	0.4977
✓	✗	0.3378	0.2145	0.5826	0.4867
✓	✓	0.3536	0.2295	0.5908	0.5190

(b) Ablation study of modalities.

Modality			NLG		CE	
ECG	CXR	LAB	MET.	ROU.	REC.	F1
✗	✓	✓	0.3245	0.2058	0.5320	0.4739
✓	✗	✓	0.3267	0.2019	0.5739	0.4869
✓	✓	✗	0.3455	0.2218	0.5845	0.5023
✓	✓	✓	0.3536	0.2295	0.5908	0.5190

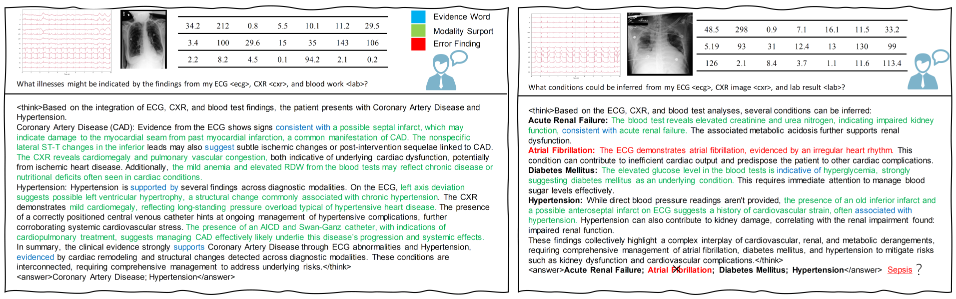

Figure 4: Inference examples of MedTVT-R1. Left: successful case with accurate multimodal diagnosis; Right: failure case where coexisting cardiac, renal, and metabolic abnormalities led the model to prioritize atrial fibrillation and miss sepsis.

4.3 Qualitative Analysis

MedTVT-R1 integrates chest X-rays (CXR), electrocardiograms (ECG), and laboratory (LAB) data into coherent, evidence-supported diagnostic conclusions (Figure 4). We illustrate its behavior through one high-performing case and one complex multi-disease case from two perspectives: *Multimodal Integration* and *Evidence-Based Reasoning*. **1) Multimodal Integration.** In a high-performing case (*Coronary Artery Disease*, *Hypertension*), complementary ECG, CXR, and LAB findings align to reinforce diagnoses, with cross-modal evidence yielding precise and clinically consistent results. The right panel illustrates a complex failure case under interference from multiple coexisting diseases: when cardiac, renal, and metabolic abnormalities occur simultaneously, the model tends to prioritize high-confidence conditions and overlook acute or subtle ones. Here, ECG findings of "irregular rhythm" and absent P waves led to an atrial fibrillation diagnosis, resulting in a missed sepsis diagnosis. Such situations, arising from limited supporting modality evidence, may benefit from incorporating additional modalities to strengthen the evidence chain. **2) Evidence-Based Reasoning.** In the high-performing case, the model explicitly links features across modalities—e.g., ECG-derived left ventricular hypertrophy with CXR cardiac enlargement—to justify conclusions. In the complex case, reasoning is dominated by strong single-modality cues, underscoring the potential of expanded multimodal inputs to improve cross-modal reasoning consistency. These examples highlight MedTVT-R1's strength in synthesizing heterogeneous clinical evidence, while complex scenarios reveal opportunities to enhance diagnostic coverage through richer multimodal evidence.

5 Conclusion

In conclusion, the proposed MedTVT-R1 framework represents a significant advancement in the application of multimodal large language models (MLLMs) for medical diagnosis. By integrating the complementary strengths of ECG, CXR, and LAB data, MedTVT-R1 addresses the limitations of single-modal approaches and provides a more holistic understanding of complex diseases. The innovative MedTVT-QA dataset facilitates physiological perception and multi-disease diagnosis by leveraging a Chain of Evidence strategy. Additionally, the modality perception layer enhances cross-modal interactions, while Reinforcement Fine-Tuning with Group Relative Policy Optimization and the Jaccard Reward boosts precision and reliability in diagnosis capabilities. Extensive experiments validate MedTVT-R1's superior performance in both physiological-level understanding and disease-level diagnosis, highlighting its potential for practical clinical applications, such as interpretable diagnostic report generation and complex comorbidity reasoning.

REFERENCES

Mohammed Abdelaziz, Tianfu Wang, and Ahmed Elazab. Alzheimer's disease diagnosis framework from incomplete multimodal data using convolutional neural networks. *Journal of biomedical informatics*, 121:103863, 2021.

Josh Achiam, Steven Adler, Sandhini Agarwal, Lama Ahmad, Ilge Akkaya, Florencia Leoni Aleman, Diogo Almeida, Janko Altenschmidt, Sam Altman, Shyamal Anadkat, et al. Gpt-4 technical report. *arXiv preprint arXiv:2303.08774*, 2023.

Juan Miguel Lopez Alcaraz and Nils Strodthoff. Cardiolab: Laboratory values estimation and monitoring from electrocardiogram signals–a multimodal deep learning approach. *arXiv preprint arXiv:2411.14886*, 2024.

Yaqoob Ansari, Omar Mourad, Khalid Qaraqe, and Erchin Serpedin. Deep learning for ecg arrhythmia detection and classification: an overview of progress for period 2017–2023. *Frontiers in Physiology*, 14:1246746, 2023.

Shuai Bai, Keqin Chen, Xuejing Liu, Jialin Wang, Wenbin Ge, Sibo Song, Kai Dang, Peng Wang, Shijie Wang, Jun Tang, et al. Qwen2. 5-vl technical report. *arXiv preprint arXiv:2502.13923*, 2025.

Aleksa Bisercic, Mladen Nikolic, Mihaela van der Schaar, Boris Delibasic, Pietro Lio, and Andrija Petrovic. Interpretable medical diagnostics with structured data extraction by large language models. *arXiv preprint arXiv:2306.05052*, 2023.

Erdi Çallı, Ecem Sogancioglu, Bram van Ginneken, Kicky G van Leeuwen, and Keelin Murphy. Deep learning for chest x-ray analysis: A survey. *Medical image analysis*, 72:102125, 2021.

Andrew Cassar, David R Holmes Jr, Charanjit S Rihal, and Bernard J Gersh. Chronic coronary artery disease: diagnosis and management. In *Mayo Clinic Proceedings*, volume 84, pp. 1130–1146. Elsevier, 2009.

Junying Chen, Chi Gui, Ruyi Ouyang, Anningzhe Gao, Shunian Chen, Guiming Hardy Chen, Xidong Wang, Ruifei Zhang, Zhenyang Cai, Ke Ji, et al. Huatuogpt-vision, towards injecting medical visual knowledge into multimodal llms at scale. *arXiv preprint arXiv:2406.19280*, 2024a.

Xin Chen, Yanxiang Niu, Jianqi Fan, Lu Lu, and Haojun Fan. Ecg-based intelligent model for coronary heart disease screening. In *Proceedings of the 2024 11th International Conference on Biomedical and Bioinformatics Engineering*, pp. 72–77, 2024b.

Alan Dao and Dinh Bach Vu. Alphamaze: Enhancing large language models' spatial intelligence via grpo. *arXiv preprint arXiv:2502.14669*, 2025.

Matt Deitke, Christopher Clark, Sangho Lee, Rohun Tripathi, Yue Yang, Jae Sung Park, Mohammadreza Salehi, Niklas Muennighoff, Kyle Lo, Luca Soldaini, et al. Molmo and pixmo: Open weights and open data for state-of-the-art multimodal models. *arXiv preprint arXiv:2409.17146*, 2024.

Alexey Dosovitskiy, Lucas Beyer, Alexander Kolesnikov, Dirk Weissenborn, Xiaohua Zhai, Thomas Unterthiner, Mostafa Dehghani, Matthias Minderer, Georg Heigold, Sylvain Gelly, et al. An image is worth 16x16 words: Transformers for image recognition at scale. *arXiv preprint arXiv:2010.11929*, 2020.

Arthur S Elstein. On the origins and development of evidence-based medicine and medical decision making. *Inflammation research*, 53:S184–S189, 2004.

Jack Gallifant, Majid Afshar, Saleem Ameen, Yindalon Aphinyanaphongs, Shan Chen, Giovanni Cacciamani, Dina Demner-Fushman, Dmitriy Dligach, Roxana Daneshjou, Chrystinne Fernandes, et al. The tripod-llm reporting guideline for studies using large language models. *Nature Medicine*, pp. 1–10, 2025.

Nafiseh Ghaffar Nia, Erkan Kaplanoglu, and Ahad Nasab. Evaluation of artificial intelligence techniques in disease diagnosis and prediction. *Discover Artificial Intelligence*, 3(1):5, 2023.

Brian Gow, Tom Pollard, Larry A Nathanson, Alistair Johnson, Benjamin Moody, Chrystinne Fernandes, Nathaniel Greenbaum, Jonathan W Waks, Parastou Eslami, Tanner Carbonati, et al. Mimic-iv-ecg: Diagnostic electrocardiogram matched subset. *Type: dataset*, 6:13–14, 2023.

Aaron Grattafiori, Abhimanyu Dubey, Abhinav Jauhri, Abhinav Pandey, Abhishek Kadian, Ahmad Al-Dahle, Aiesha Letman, Akhil Mathur, Alan Schelten, Alex Vaughan, et al. The llama 3 herd of models. *arXiv preprint arXiv:2407.21783*, 2024.

Sanjana Gundapaneni, Zhuo Zhi, and Miguel Rodrigues. Deep learning-based noninvasive screening of type 2 diabetes with chest x-ray images and electronic health records. *arXiv preprint arXiv:2412.10955*, 2024.

Daya Guo, Dejian Yang, Haowei Zhang, Junxiao Song, Ruoyu Zhang, Runxin Xu, Qihao Zhu, Shirong Ma, Peiyi Wang, Xiao Bi, et al. Deepseek-r1: Incentivizing reasoning capability in llms via reinforcement learning. *arXiv preprint arXiv:2501.12948*, 2025.

Mikel Hernandez, Gorka Epelde, Ane Alberdi, Rodrigo Cilla, and Debbie Rankin. Synthetic data generation for tabular health records: A systematic review. *Neurocomputing*, 493:28–45, 2022.

Edward J Hu, Yelong Shen, Phillip Wallis, Zeyuan Allen-Zhu, Yuanzhi Li, Shean Wang, Lu Wang, Weizhu Chen, et al. Lora: Low-rank adaptation of large language models. *ICLR*, 1(2):3, 2022.

Jingwei Huang, Donghan M Yang, Ruichen Rong, Kuroush Nezafati, Colin Treager, Zhikai Chi, Shidan Wang, Xian Cheng, Yujia Guo, Laura J Klesse, et al. A critical assessment of using chatgpt for extracting structured data from clinical notes. *npj Digital Medicine*, 7(1):106, 2024.

Jeremy Irvin, Pranav Rajpurkar, Michael Ko, Yifan Yu, Silviana Ciurea-Ilcus, Chris Chute, Henrik Marklund, Behzad Haghgoo, Robyn Ball, Katie Shpanskaya, et al. Chexpert: A large chest radiograph dataset with uncertainty labels and expert comparison. In *Proceedings of the AAAI conference on artificial intelligence*, volume 33, pp. 590–597, 2019.

Mingyu Jin, Qinkai Yu, Chong Zhang, Dong Shu, Suiyuan Zhu, Mengnan Du, Yongfeng Zhang, and Yanda Meng. Health-llm: Personalized retrieval-augmented disease prediction model. *arXiv preprint arXiv:2402.00746*, 10, 2024.

Alistair Johnson, Lucas Bulgarelli, Tom Pollard, Steven Horng, Leo Anthony Celi, and Roger Mark. Mimic-iv. *PhysioNet. Available online at: https://physionet. org/content/mimiciv/1.0/(accessed August 23, 2021)*, pp. 49–55, 2020.

Alistair EW Johnson, Tom J Pollard, Nathaniel R Greenbaum, Matthew P Lungren, Chih-ying Deng, Yifan Peng, Zhiyong Lu, Roger G Mark, Seth J Berkowitz, and Steven Horng. Mimic-cxr-jpg, a large publicly available database of labeled chest radiographs. *arXiv preprint arXiv:1901.07042*, 2019.

Adrienne Kline, Hanyin Wang, Yikuan Li, Saya Dennis, Meghan Hutch, Zhenxing Xu, Fei Wang, Feixiong Cheng, and Yuan Luo. Multimodal machine learning in precision health: A scoping review. *npj Digital Medicine*, 5(1):171, 2022.

Anil Kumar. Deep learning for multi-modal medical imaging fusion: Enhancing diagnostic accuracy in complex disease detection. *Int J Eng Technol Res Manag*, 6(11):183, 2022.

Yuxiang Lai, Jike Zhong, Ming Li, Shitian Zhao, and Xiaofeng Yang. Med-r1: Reinforcement learning for generalizable medical reasoning in vision-language models. *arXiv preprint arXiv:2503.13939*, 2025.

Xiang Lan, Feng Wu, Kai He, Qinghao Zhao, Shenda Hong, and Mengling Feng. Gem: Empowering mllm for grounded ecg understanding with time series and images. *arXiv preprint arXiv:2503.06073*, 2025.

Seowoo Lee, Jiwon Youn, Hyungjin Kim, Mansu Kim, and Soon Ho Yoon. Cxr-llava: a multimodal large language model for interpreting chest x-ray images. *European Radiology*, pp. 1–13, 2025.

Suhyeon Lee, Won Jun Kim, Jinho Chang, and Jong Chul Ye. Llm-cxr: instruction-finetuned llm for cxr image understanding and generation. *arXiv preprint arXiv:2305.11490*, 2023.

Bo Li, Kaichen Zhang, Hao Zhang, Dong Guo, Renrui Zhang, Feng Li, Yuanhan Zhang, Ziwei Liu, and Chunyuan Li. Llava-next: Stronger llms supercharge multimodal capabilities in the wild, May 2024a. URL https://llava-vl.github.io/blog/2024-05-10-llava-next-stronger-llms/.

Bo Li, Yuanhan Zhang, Dong Guo, Renrui Zhang, Feng Li, Hao Zhang, Kaichen Zhang, Peiyuan Zhang, Yanwei Li, Ziwei Liu, et al. Llava-onevision: Easy visual task transfer. *arXiv preprint arXiv:2408.03326*, 2024b.

Cheng-Yi Li, Kao-Jung Chang, Cheng-Fu Yang, Hsin-Yu Wu, Wenting Chen, Hritik Bansal, Ling Chen, Yi-Ping Yang, Yu-Chun Chen, Shih-Pin Chen, et al. Towards a holistic framework for multimodal llm in 3d brain ct radiology report generation. *Nature Communications*, 16(1):2258, 2025.

Chunyuan Li, Cliff Wong, Sheng Zhang, Naoto Usuyama, Haotian Liu, Jianwei Yang, Tristan Naumann, Hoifung Poon, and Jianfeng Gao. Llava-med: Training a large language-and-vision assistant for biomedicine in one day. *Advances in Neural Information Processing Systems*, 36: 28541–28564, 2023a.

Chunyuan Li, Cliff Wong, Sheng Zhang, Naoto Usuyama, Haotian Liu, Jianwei Yang, Tristan Naumann, Hoifung Poon, and Jianfeng Gao. Llava-med: Training a large language-and-vision assistant for biomedicine in one day. *Advances in Neural Information Processing Systems*, 36: 28541–28564, 2023b.

Valentin Liévin, Christoffer Egeberg Hother, Andreas Geert Motzfeldt, and Ole Winther. Can large language models reason about medical questions? *Patterns*, 5(3), 2024.

Chin-Sheng Lin, Yung-Tsai Lee, Wen-Hui Fang, Yu-Sheng Lou, Feng-Chih Kuo, Chia-Cheng Lee, and Chin Lin. Deep learning algorithm for management of diabetes mellitus via electrocardiogram-based glycated hemoglobin (ecg-hba1c): a retrospective cohort study. *Journal of Personalized Medicine*, 11(8):725, 2021.

Chang Liu, Yuanhe Tian, Weidong Chen, Yan Song, and Yongdong Zhang. Bootstrapping large language models for radiology report generation. In *Proceedings of the AAAI Conference on Artificial Intelligence*, volume 38, pp. 18635–18643, 2024a.

Haotian Liu, Chunyuan Li, Qingyang Wu, and Yong Jae Lee. Visual instruction tuning. *Advances in neural information processing systems*, 36:34892–34916, 2023.

Haotian Liu, Chunyuan Li, Yuheng Li, and Yong Jae Lee. Improved baselines with visual instruction tuning. In *Proceedings of the IEEE/CVF Conference on Computer Vision and Pattern Recognition*, pp. 26296–26306, 2024b.

Shansong Liu, Atin Sakkeer Hussain, Qilong Wu, Chenshuo Sun, and Ying Shan. Mumu-llama: Multi-modal music understanding and generation via large language models. *arXiv preprint arXiv:2412.06660*, 2024c.

Xinwen Liu, Huan Wang, Zongjin Li, and Lang Qin. Deep learning in ecg diagnosis: A review. *Knowledge-Based Systems*, 227:107187, 2021.

Ziyu Liu, Zeyi Sun, Yuhang Zang, Xiaoyi Dong, Yuhang Cao, Haodong Duan, Dahua Lin, and Jiaqi Wang. Visual-rft: Visual reinforcement fine-tuning. *arXiv preprint arXiv:2503.01785*, 2025.

Haoyu Lu, Wen Liu, Bo Zhang, Bingxuan Wang, Kai Dong, Bo Liu, Jingxiang Sun, Tongzheng Ren, Zhuoshu Li, Hao Yang, et al. Deepseek-vl: towards real-world vision-language understanding. *arXiv preprint arXiv:2403.05525*, 2024a.

Ming Y Lu, Bowen Chen, Drew FK Williamson, Richard J Chen, Melissa Zhao, Aaron K Chow, Kenji Ikemura, Ahrong Kim, Dimitra Pouli, Ankush Patel, et al. A multimodal generative ai copilot for human pathology. *Nature*, 634(8033):466–473, 2024b.

Michael Moor, Qian Huang, Shirley Wu, Michihiro Yasunaga, Yash Dalmia, Jure Leskovec, Cyril Zakka, Eduardo Pontes Reis, and Pranav Rajpurkar. Med-flamingo: a multimodal medical few-shot learner. In *Machine Learning for Health (ML4H)*, pp. 353–367. PMLR, 2023.

Jiazhen Pan, Che Liu, Junde Wu, Fenglin Liu, Jiayuan Zhu, Hongwei Bran Li, Chen Chen, Cheng Ouyang, and Daniel Rueckert. Medvlm-r1: Incentivizing medical reasoning capability of vision-language models (vlms) via reinforcement learning. *arXiv preprint arXiv:2502.19634*, 2025.

Shyam Sundhar Ramesh, Yifan Hu, Iason Chaimalas, Viraj Mehta, Pier Giuseppe Sessa, Haitham Bou Ammar, and Ilija Bogunovic. Group robust preference optimization in reward-free rlhf. *Advances in Neural Information Processing Systems*, 37:37100–37137, 2024.

Adriel Saporta, Aahlad Manas Puli, Mark Goldstein, and Rajesh Ranganath. Contrasting with symile: Simple model-agnostic representation learning for unlimited modalities. *Advances in Neural Information Processing Systems*, 37:56919–56957, 2024.

John Schulman, Filip Wolski, Prafulla Dhariwal, Alec Radford, and Oleg Klimov. Proximal policy optimization algorithms. *arXiv preprint arXiv:1707.06347*, 2017.

Zhihong Shao, Peiyi Wang, Qihao Zhu, Runxin Xu, Junxiao Song, Xiao Bi, Haowei Zhang, Mingchuan Zhang, YK Li, Y Wu, et al. Deepseekmath: Pushing the limits of mathematical reasoning in open language models. *arXiv preprint arXiv:2402.03300*, 2024.

Junjie Shentu and Noura Al Moubayed. Cxr-irgen: an integrated vision and language model for the generation of clinically accurate chest x-ray image-report pairs. In *Proceedings of the IEEE/CVF Winter Conference on Applications of Computer Vision*, pp. 5212–5221, 2024.

Sandra Steyaert, Marija Pizurica, Divya Nagaraj, Priya Khandelwal, Tina Hernandez-Boussard, Andrew J Gentles, and Olivier Gevaert. Multimodal data fusion for cancer biomarker discovery with deep learning. *Nature machine intelligence*, 5(4):351–362, 2023.

N. Strodthoff, J. M. Lopez Alcaraz, and W. Haverkamp. Mimic-iv-ecg-ext-icd: Diagnostic labels for mimic-iv-ecg (version 1.0.1). *PhysioNet*, 2024.

Md Shaheenur Islam Sumon, Md Sakib Bin Islam, Md Sohanur Rahman, Md Sakib Abrar Hossain, Amith Khandakar, Anwarul Hasan, M Murugappan, and Muhammad EH Chowdhury. Cardiotabnet: A novel hybrid transformer model for heart disease prediction using tabular medical data. *arXiv preprint arXiv:2503.17664*, 2025.

Huajie Tan, Yuheng Ji, Xiaoshuai Hao, Minglan Lin, Pengwei Wang, Zhongyuan Wang, and Shanghang Zhang. Reason-rft: Reinforcement fine-tuning for visual reasoning. *arXiv preprint arXiv:2503.20752*, 2025.

Ryutaro Tanno, David GT Barrett, Andrew Sellergren, Sumedh Ghaisas, Sumanth Dathathri, Abigail See, Johannes Welbl, Charles Lau, Tao Tu, Shekoofeh Azizi, et al. Collaboration between clinicians and vision–language models in radiology report generation. *Nature Medicine*, 31(2):599–608, 2025.

Yuanyuan Tian, Zhiyuan Li, Yanrui Jin, Mengxiao Wang, Xiaoyang Wei, Liqun Zhao, Yunqing Liu, Jinlei Liu, and Chengliang Liu. Foundation model of ecg diagnosis: Diagnostics and explanations of any form and rhythm on ecg. *Cell Reports Medicine*, 5(12), 2024.

Zeyue Tian, Yizhu Jin, Zhaoyang Liu, Ruibin Yuan, Xu Tan, Qifeng Chen, Wei Xue, and Yike Guo. Audiox: Diffusion transformer for anything-to-audio generation. *arXiv preprint arXiv:2503.10522*, 2025.

Janani Venugopalan, Li Tong, Hamid Reza Hassanzadeh, and May D Wang. Multimodal deep learning models for early detection of alzheimer's disease stage. *Scientific reports*, 11(1):3254, 2021.

Shengqiong Wu, Hao Fei, Leigang Qu, Wei Ji, and Tat-Seng Chua. Next-gpt: Any-to-any multimodal llm. In *Forty-first International Conference on Machine Learning*, 2024.

Kai Yang, Massimo Hong, Jiahuan Zhang, Yizhen Luo, Suyuan Zhao, Ou Zhang, Xiaomao Yu, Jiawen Zhou, Liuqing Yang, Ping Zhang, et al. Ecg-lm: Understanding electrocardiogram with a large language model. *Health Data Science*, 5:0221, 2025.

Wenfang Yao, Chen Liu, Kejing Yin, William Cheung, and Jing Qin. Addressing asynchronicity in clinical multimodal fusion via individualized chest x-ray generation. *Advances in Neural Information Processing Systems*, 37:29001–29028, 2024.

Chao Yu, Akash Velu, Eugene Vinitsky, Jiaxuan Gao, Yu Wang, Alexandre Bayen, and Yi Wu. The surprising effectiveness of ppo in cooperative multi-agent games. *Advances in neural information processing systems*, 35:24611–24624, 2022.

Han Yu, Peikun Guo, and Akane Sano. Zero-shot ecg diagnosis with large language models and retrieval-augmented generation. In *Machine learning for health (ML4H)*, pp. 650–663. PMLR, 2023.

Dong Yuan, Eti Rastogi, Gautam Naik, Sree Prasanna Rajagopal, Sagar Goyal, Fen Zhao, Bharath Chintagunta, and Jeff Ward. A continued pretrained llm approach for automatic medical note generation. *arXiv preprint arXiv:2403.09057*, 2024.

Hang Zhang, Xin Li, and Lidong Bing. Video-llama: An instruction-tuned audio-visual language model for video understanding. *arXiv preprint arXiv:2306.02858*, 2023.

Yubao Zhao, Tian Zhang, Xu Wang, Puyu Han, Tong Chen, Linlin Huang, Youzhu Jin, and Jiaju Kang. Ecg-chat: A large ecg-language model for cardiac disease diagnosis. *arXiv preprint arXiv:2408.08849*, 2024.

Yuze Zhao, Jintao Huang, Jinghan Hu, Xingjun Wang, Yunlin Mao, Daoze Zhang, Zeyinzi Jiang, Zhikai Wu, Baole Ai, Ang Wang, et al. Swift: a scalable lightweight infrastructure for fine-tuning. In *Proceedings of the AAAI Conference on Artificial Intelligence*, volume 39, pp. 29733–29735, 2025.

Jinguo Zhu, Weiyun Wang, Zhe Chen, Zhaoyang Liu, Shenglong Ye, Lixin Gu, Yuchen Duan, Hao Tian, Weijie Su, Jie Shao, et al. Internvl3: Exploring advanced training and test-time recipes for open-source multimodal models. *arXiv preprint arXiv:2504.10479*, 2025.

APPENDIX

A DETAILS ABOUT THE PROMPTS OF MEDTVT-QA'S CONSTRUCTION

This section presents the detailed prompts used in constructing the MedTVT-QA dataset.

ECG-QA Prompt

***Role Setting*:** You are a renowned cardiologist with expertise in interpreting electrocardiograms (ECGs).
***Task Description*:** The ECG analysis has yielded the following labels: {`labels`}. Based on these labels, please address the question: {`question`}.
***Answer Guidance*:** Your response should incorporate all relevant labels, excluding any unrelated ones. Provide a synthesis of the labels, focusing on clinical significance.
***Answer Format*:** Begin with a brief introduction to your analysis. Provide detailed explanations for each specific ECG label. Offer a concise summary.

CXR-QA Prompt

***Role Setting*:** You are a radiology expert with expertise in interpreting chest X-ray image.
***Task Description*:** The chest X-ray report is given {`report`} Base on the given chest X-ray report, answer the question {`question`}
***Answer Guidance*:** Describe the overall condition of the lungs, heart, and chest cavity in the image. Identify and explain any abnormal findings such as shadows, opacities, effusions, or masses. Provide possible diagnoses.

LAB-QA Prompt

***Role Setting*:** Please analyze this set of blood test data as a medical professional.
***Task Description*:** This is the question: {`question`} The following are the lab data: ”Hematocrit”: {`data[0]`}; ”Platelet Count”: {`data[1]`}; ”Creatinine”: {`data[2]`}; ”Potassium”: {`data[3]`}; ”Hemoglobin”: {`data[4]`}; ”White Blood Cells”: {`data[5]`}; ”MCHC”: {`data[6]`}; ”Red Blood Cells”: {`data[7]`}; ”MCV”: {`data[8]`}; ”MCH”: {`data[9]`}; ”RDW”: {`data[10]`}; ”Urea Nitrogen”: {`data[11]`}; ”Sodium”: {`data[12]`}; ”Chloride”: {`data[13]`}; ”Bicarbonate”: {`data[14]`}; ”Anion Gap”: {`data[15]`}; ”Glucose”: {`data[16]`}; ”Magnesium”: {`data[17]`}; ”Calcium, Total”: {`data[18]`}; ”Phosphate”: {`data[19]`}; ”INR(PT)”: {`data[20]`}; ”PT”: {`data[21]`}; ”PTT”: {`data[22]`}; ”Basophils”: {`data[23]`}; ”Neutrophils”: {`data[24]`}; ”Monocytes”: {`data[25]`}; ”Eosinophils”: {`data[26]`}; ”Lymphocytes”: {`data[27]`}; ”RDW-SD”: {`data[28]`}; ”H”: {`data[29]`}; ”L”: {`data[30]`}; ”I”: {`data[31]`}; ”Alanine Aminotransferase (ALT)”: {`data[32]`}; ”Asparate Aminotransferase (AST)”: {`data[33]`}; ”Lactate”: {`data[34]`}; ”Alkaline Phosphatase”: {`data[35]`}; ”Bilirubin, Total”: {`data[36]`}; ”pH”: {`data[37]`}; ”Albumin”: {`data[38]`}; ”Base Excess”: {`data[39]`}; ”pO2”: {`data[40]`} ”Calculated Total CO2”: {`data[41]`}; ”pCO2”: {`data[42]`}; ”Absolute Neutrophil Count”: {`data[43]`}; ”Absolute Eosinophil Count”: {`data[44]`}; ”Absolute Monocyte Count”: {`data[45]`}; ”Absolute Basophil Count”: {`data[46]`}; ”Absolute Lymphocyte Count”: {`data[47]`}; ”Creatine Kinase (CK)”: {`data[48]`} ”Immature Granulocytes”: {`data[49]`}
***Answer Guidance*:** These data comprise 50 different indicators, categorized into seven main classes: routine blood indicators, electrolyte and metabolic indicators, renal function indicators, liver function indicators, acid-base balance and gas exchange, coagulation function indicators, and other indicators.
***Answer Format*:** Begin with a brief introduction to your analysis.
routine blood indicators: explanation
electrolyte and metabolic indicators: explanation
renal function indicators: explanation
liver function indicators: explanation
acid-base balance and gas exchange: explanation
coagulation function indicators: explanation
other indicators: explanation
Finally, offer a concise summary.

Disease-QA Prompt

***Role Setting*:** You are a renowned diagnostician with expertise in integrating ECG, CXR, and blood test results.
***Task Description*:** The following diagnostics have been provided:
- ECG Analysis: {`ecg_report`}
- CXR Analysis: {`cxr_report`}
- Blood Test Analysis: {`blood_test_report`}
- Diseases: {`result_diseases`}

You need to pretend that the ECG, CXR, and blood test analyses are based on your interpretation of the raw data, and the final diagnosis is your synthesis of these three diagnostic methods, please address the question: {`question`}
***Answer Guidance*:** Please find definitive evidence from the ECG, CXR, and blood test results, leveraging the complementarity and mutual corroboration of these three modalities, to robustly prove the reasons why the patient has the diseases I provided. Your response must include every disease I provided, using the exact wording I provided, and you must not mention any diseases other than those I provided. Please make sure to provide evidence for these diagnoses! These are confirmed conditions.
***Answer Format*:** <think>{Diagnostic evidence synthesized from the three modalities}</think>\n <answer>{disease1; disease2; ...}</answer>

B LABEL DISTRIBUTION OF MEDTVT-QA

When constructing the physiology-level ECG-QA dataset, we filtered out invalid ECG labels to ensure that the final labels align with morphology descriptions at the physiological level. Additionally, we conducted a detailed statistical analysis of the labels in the ECG-QA training data. As shown in Table 5, it presents ECG labels with occurrences greater than 100 along with their respective counts.

Table 5: ECG Labels and Counts (¿100) in ECG-QA.

Label	Count
sinus rhythm with 1st degree a-v block	140
sinus rhythm	4033
atrial fibrillation	761
sinus tachycardia	1565
consider acute st elevation mi	161
atrial fibrillation with rapid ventricular response	224
age not entered, assumed to be 50 years old for purpose of ecg interpretation	328
sinus bradycardia	402
sinus rhythm with pac(s)	132
sinus rhythm with borderline 1st degree a-v block	121
pacemaker rhythm - no further analysis	160
leftward axis	435
possible left anterior fascicular block	138
rightward axis	164
probable left atrial enlargement	224
low qrs voltages in precordial leads	540
st junctional depression is nonspecific	149
possible inferior infarct - age undetermined	425
lateral t wave changes are nonspecific	328
short pr interval	167
inferior t wave changes are nonspecific	312
left ventricular hypertrophy	428
lvh with secondary repolarization abnormality	285
left axis deviation	1067
poor r wave progression - probable normal variant	538
indeterminate axis	108
possible anterior infarct - age undetermined	511
anterior t wave changes are nonspecific	182
possible left atrial abnormality	271
inferior/lateral st-t changes are nonspecific	240
prolonged qt interval	618
possible anteroseptal infarct - age undetermined	254
septal t wave changes are nonspecific	134
right bundle branch block	517
lateral st-t changes are nonspecific	289
anteroseptal infarct - age undetermined	129
left anterior fascicular block	202

Label	Count
extensive st-t changes are nonspecific	111
inferior infarct - age undetermined	550
rsr'(v1) - probable normal variant	199
left bundle branch block	354
low qrs voltages in limb leads	395
extensive st-t changes may be due to myocardial ischemia	143
possible left ventricular hypertrophy	150
abnormal r-wave progression, early transition	102
inferior infarct, old	123
ventricular premature complex	119
possible septal infarct - age undetermined	188
right axis deviation	141
lateral st-t changes may be due to myocardial ischemia	227
inferior/lateral st-t changes may be due to myocardial ischemia	167
iv conduction defect	376
generalized low qrs voltages	161
qrs changes v3/v4 may be due to lvh but cannot rule out anterior infarct	103
lateral t wave changes may be due to myocardial ischemia	106
rbbb with left anterior fascicular block	314
extensive st-t changes may be due to hypertrophy and/or ischemia	135
normal ecg	753
normal ecg except for rate	334
abnormal ecg	4761
borderline ecg	2074
inferior/lateral st-t changes may be due to hypertrophy and/or ischemia	116
lateral st-t changes may be due to hypertrophy and/or ischemia	112

Figure 5 presents an example report from the MIMIC-IV-CXR dataset, used in constructing CXR-QA. The report contains some unclear and unrelated content to the CXR image description. By applying the previously described CXR prompts, we transformed the report into a more organized and focused description centered on CXR.

Figure 5: An CXR report example from MIMIX-IV-CXR-report dataset.

FINAL REPORT

EXAMINATION: CHEST (PA AND LAT)
INDICATION: ___F with new onset asciteps // eval for infection

TECHNIQUE: Chest PA and lateral

COMPARISON: None.

FINDINGS: There is no focal consolidation, pleural effusion or pneumothorax. Bilateral nodular opacities that most likely represent nipple shadows.

The cardiomediastinal silhouette is normal. Clips project over the left lung, potentially within the breast. The imaged upper abdomen is unremarkable. Chronic deformity of the posterior left sixth and seventh ribs are noted.
IMPRESSION: No acute cardiopulmonary process.

Disease-level labels are derived from the MIMIC-IV-ECG-EXT-ICD (Strodthoff et al., 2024) dataset, with these labels stored as ICD-10 codes. Each sample may correspond to multiple disease categories. We filtered out diseases for which evidence could not be found in ECG, CXR, or LAB data. Ultimately, we identified seven main categories: Coronary Artery Disease, Acute Renal Failure, Hypertension, Atrial Fibrillation, Pneumonia, Diabetes Mellitus, and Sepsis, along with some subclasses within these categories. Details are provided in Table 6.

Table 6: ICD-10 Disease Statistics with Corresponding Counts.

Disease Category	ICD-10 Code	Count
Coronary Artery Disease		
Coronary Artery Disease	I2510	2680
Chronic ischemic heart disease, unspecified	I252	936
Atherosclerotic heart disease of native coronary artery	I259	190
Other forms of chronic ischemic heart disease	I253	8
Ischemic cardiomyopathy	I255	79
Acute Renal Failure		
Acute kidney failure, unspecified	N179	2379
Acute kidney failure with tubular necrosis	N170	689

Disease Category	**ICD-10 Code**	**Count**
Acute kidney failure with other specified morphologic lesions	N178	12
Acute kidney failure with acute cortical necrosis	N171	1
Hypertension		
Essential (primary) hypertension	I10	4155
Hypertensive heart and chronic kidney disease, unspecified	I129	1536
Hypertensive heart disease with heart failure	I120	515
Hypertensive heart and chronic kidney disease with heart failure	I130	119
Hypertensive heart disease without heart failure	I110	77
Hypertensive heart and chronic kidney disease with heart failure and stage 5 CKD or ESRD	I132	37
Hypertensive heart disease, unspecified	I119	8
Other secondary hypertension	I159	1
Renovascular hypertension	I150	7
Other specified secondary hypertension	I158	1
Atrial Fibrillation		
Persistent atrial fibrillation	I4891	2623
Permanent atrial fibrillation	I4892	317
Paroxysmal atrial fibrillation	I480	237
Other specified atrial fibrillation	I482	104
Atrial flutter, unspecified	I481	15
Typical atrial flutter	I483	1
Atypical atrial flutter	I484	1
Pneumonia		
Pneumonia, unspecified organism	J189	1442
Pneumonia due to other specified bacteria	J181	25
Pneumonia due to Haemophilus influenzae	J188	18
Pneumonia due to Klebsiella pneumoniae	J180	5
Diabetes Mellitus		
Type 2 diabetes mellitus without complications	E119	1752
Type 2 diabetes mellitus with unspecified complications	E1129	217
Type 2 diabetes mellitus with hyperglycemia	E11319	296
Type 2 diabetes mellitus with renal complications	E1140	348
Type 2 diabetes mellitus with circulatory complications	E1165	360
Type 2 diabetes mellitus with other specified complications	E118	29
Type 2 diabetes mellitus with unspecified complications	E139	29
Type 1 diabetes mellitus without complications	E109	27
Type 1 diabetes mellitus with unspecified complications	E138	2
Type 1 diabetes mellitus with other specified complications	E108	3
Sepsis		
Sepsis, unspecified organism	A419	1088
Severe sepsis without septic shock	R6520	939
Severe sepsis with septic shock	R6521	873
Sepsis due to Streptococcus pneumoniae	A403	26
Sepsis due to Escherichia coli	A412	2
Sepsis due to other Gram-negative organisms	A409	69
Sepsis due to anaerobes	A414	28
Sepsis due to other specified bacteria	A411	26
Sepsis due to Staphylococcus aureus	A401	3
Sepsis due to other specified Staphylococcus	A408	4
Sepsis due to other specified bacteria	A413	1
Sepsis due to unspecified Staphylococcus	A400	2

C Examples of QA Pairs Corresponding to Each Modality

This section provides examples of question-answer pairs corresponding to each modality (e.g., ECG, CXR, LAB) in the MedTVT-QA dataset.

ECG-QA Example

***Question*:** What information can be derived from the ECG ¡ecg¿?
***Answer*:** ECG Analysis: Upon evaluating the electrocardiogram (ECG), the following observations can be made:
1.Sinus Rhythm: The heart is under the control of the sinoatrial (SA) node, which is the natural pacemaker. This finding suggests that the electrical activity of the heart is originating from the SA node and progressing through the normal conduction pathway, leading to a regular rhythm. This is a foundational indicator of organized cardiac activity.
2. Left Bundle Branch Block (LBBB): There is evidence of delayed or disrupted conduction through the left bundle of the heart's electrical conduction system. This results in a characteristic pattern on the ECG, with a widened QRS complex (¿120 ms) and specific morphologies in leads, such as a broad, notched appearance in V5-V6 and an absence of normal septal depolarization. LBBB may occur in conditions like ischemic heart disease, cardiomyopathy, or hypertension-induced structural changes, though it can also occasionally be found in asymptomatic individuals.
Summary: The heart demonstrates a sinus rhythm, indicating normal initiation of electrical activity. However, the presence of a left bundle branch block signifies an abnormality in electrical conduction, often associated with underlying cardiac pathology. As a whole, this ECG is classified as abnormal due to the conduction disturbance, warranting further investigation to assess structural or functional cardiac issues.

CXR-QA Example

***Question*:** Would you mind explaining the findings on my chest X-ray ¡cxr¿?
***Answer*:** Based on the evaluation of your chest X-ray image, the lungs appear overall unchanged from prior assessments, indicating no new substantial developments. There is no evidence of acute cardiopulmonary disease, which means there are no significant new concerns regarding your heart or lungs. Specifically, there are no signs of pneumonia, which would typically appear as clouded or consolidated areas in the lung fields. Similarly, there is no vascular congestion; this would generally be associated with heart-related problems affecting the lung's blood vessels and is absent in this image. Additionally, there is no pleural effusion, which would be fluid accumulation in the space between the lungs and chest wall.
However, there is a notable finding of a dense streak of atelectasis at the left base of the lung, which is a condition where a part of the lung collapses or does not inflate properly, resulting in that portion not being fully functional. This streak appears denser than usual tissue, indicating that a segment of the lung at the left base may not be fully expanded or aerated. Atelectasis can result from various causes, such as mucus blocking an airway, external pressure on the lung, or post-surgical changes.
Despite this abnormality, the absence of acute cardiopulmonary disease indicators is reassuring. The streak of atelectasis should be monitored, and clinical correlation with your symptoms is important. Continuous observation or additional imaging might be recommended to ensure there are no underlying issues contributing to this finding. Always consult with your healthcare provider to discuss the implications of these findings based on your clinical history and symptoms.

LAB-QA Example

***Question*:** Would you be able to undertake a comprehensive examination of this patient's blood panel ¡lab¿, including the reference ranges and clinical implications associated with all abnormal values?
***Answer*:** Comprehensive Blood Panel Analysis:This blood test reflects multiple systemic functions. I will analyze the provided values across seven categories, indicating normal findings and clinical implications for abnormal or missing data.
Routine Blood Indicators: Hematocrit, hemoglobin, red blood cells, MCV, and MCHC fall within normal ranges, suggesting typical oxygen-carrying capacity and erythrocyte health. RDW is borderline high, which could indicate subtle variability in red cell size, potentially pointing toward early nutritional deficiencies or mild anemia. Platelet count and white blood cells are normal, showing adequate clotting potential and immune activity. All differential leukocyte percentages are within normal ranges, reflecting balanced immunity.
Electrolyte and Metabolic Indicators: Potassium, sodium, magnesium, bicarbonate, and phosphate are within normal ranges, indicating balanced electrolytes and acid-base homeostasis. However, chloride is mildly low (97.0), potentially reflecting minor electrolyte imbalance or compensatory metabolic alkalosis. Glucose is significantly elevated (185.0), possibly suggesting poorly controlled diabetes mellitus or acute hyperglycemia. Lactate is elevated (4.6), which could suggest tissue hypoxia or metabolic distress. Calcium is borderline low (8.5), potentially indicating subtle hypocalcemia warranting further evaluation.
Renal Function Indicators: Creatinine is within the high-normal range, which might raise concerns for early renal insufficiency depending on age/gender. Urea nitrogen is elevated, possibly indicating dehydration, increased protein metabolism, or mild renal dysfunction.
Liver Function Indicators: ALT, AST, bilirubin, and alkaline phosphatase values are missing and assumed normal, precluding further analysis.
Acid-Base Balance and Gas Exchange: With missing pH and gas exchange values, bicarbonate is normal but anion gap is elevated (22.0), potentially indicating metabolic acidosis from lactate accumulation or unmeasured ions.
Coagulation Function Indicators: INR, PT, and PTT are missing and presumed normal, suggesting no overt coagulation abnormalities.
Other Indicators: Data gaps in albumin, base excess, and other parameters limit full metabolic insight.
Summary: Elevated glucose and lactate suggest metabolic dysregulation. Elevated urea nitrogen and borderline creatinine warrant renal assessment. Mild hypocalcemia and low chloride need further exploration. Elevated anion gap hints at underlying acidosis. Follow-up tests are recommended for confirmation and diagnosis refinement.

D FURTHER ANALYSIS

Disease Co-occurrence Structure and Error Patterns. As shown in Figure 6, the predicted co-occurrence matrix largely preserves the topology of the ground truth, recovering clinically plausible comorbidity clusters (e.g., hypertension–diabetes–coronary artery disease and hypertension–atrial fibrillation). Pairwise counts are modestly inflated in prediction, suggesting that the model leverages co-occurrence priors and tends to overproduce multi-label sets. The error profile in Figure 6 indicates systematic difficulty on lab-driven conditions. Diabetes mellitus and acute renal failure exhibit both high false positives and false negatives, pointing to unstable evidence due to missing labs, or heterogeneous diagnostic criteria. Sepsis also shows elevated false negatives, consistent with episodic onset and sparse specific biomarkers. In contrast, atrial fibrillation skews toward false negatives more than false positives, hinting at a conservative decision boundary or sensitivity to ECG noise/quality. Overall, the model learns a clinically meaningful dependency structure but occasionally substitutes co-occurrence priors for modality-specific evidence.

Dynamic Modality Weights and Disease-level Performance. To assess the behavior of the proposed dynamic modality-weighting mechanism, we visualized the learned weights for the three modalities using violin plots, as shown in Fig 7. The model assigns a broad range of weights across samples rather than converging to fixed or uniform values, indicating that reliance on each modality adapts on a per-case basis. The distributions are non-symmetric and, in some cases, multi-modal, suggesting the model can switch between modality-dominant decision modes depending on available evidence.

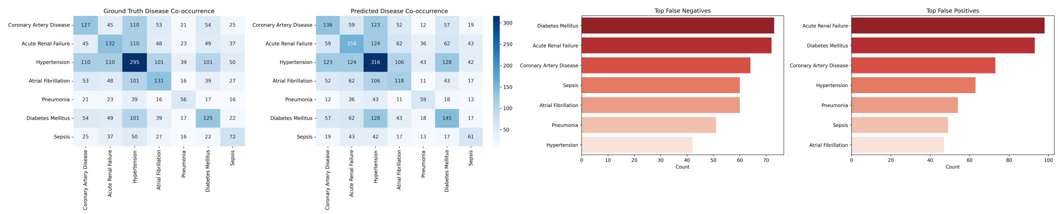

Figure 6: Disease co-occurrence and error profile. Left: Ground-truth vs. predicted co-occurrence matrices show similar structure with hypertension as a hub. Right: Top false negatives/positives highlight diabetes mellitus and acute renal failure as major sources of confusion.

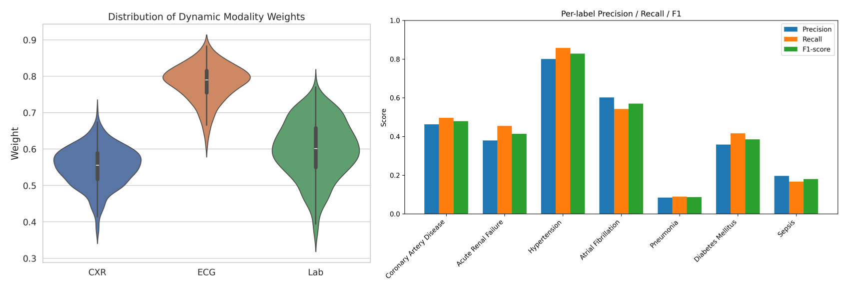

Figure 7: Dynamic modality weights and per-disease metrics. Left: Violin plots of learned weights for CXR, ECG, and Lab (median/IQR); ECG is highest and more stable, CXR lower, Lab most variable. Right: Per-label precision/recall/F1, showing alignment between higher ECG reliance and stronger cardiovascular performance, with pneumonia remaining weaker.

Linking weights to per-disease performance, the consistently higher ECG weights align with the stronger results on cardiovascular labels (e.g., hypertension and atrial fibrillation), reflecting the stable discriminative value of ECG for such conditions. CXR receives lower and less variable weights, which is consistent with the relatively weaker performance on pneumonia in our current setup—pointing to either under-exploitation of CXR features or label imbalance/noise. Lab shows the widest spread, consistent with its context-dependent value: it is more informative for organ-function–related conditions (e.g., acute renal failure) but contributes unevenly to others (e.g., sepsis, diabetes), likely due to missing tests and asynchrony.

E Performance of Various MLLMs in Handling Medical Reasoning and Diagnosis

Here, we present an example of medical analysis and diagnosis among various MLLMs and MedTVT-R1, as shown in Figure 8.

F Limitation

Although our proposed MedTVT-R1 successfully integrates CXR, ECG, and LAB data for joint multi-disease diagnosis, there are still some limitations. First, precise disease diagnosis often requires a larger volume of multimodal data collected from the same patient within a similar timeframe. However, in the short term, it is challenging to gather such large-scale data, which limits the model's generalization ability and diagnostic accuracy. Second, while our work incorporates three modalities—CXR, ECG, and LAB—more accurate disease analysis and diagnosis may rely on additional modalities, such as patient medical history, genomic data, or other biomarkers. Unfortunately, the current open-source datasets lack richer multimodal information, making such extensions difficult to achieve. Future research could aim to address these challenges to further enhance the model's diagnostic capabilities and practical applicability.

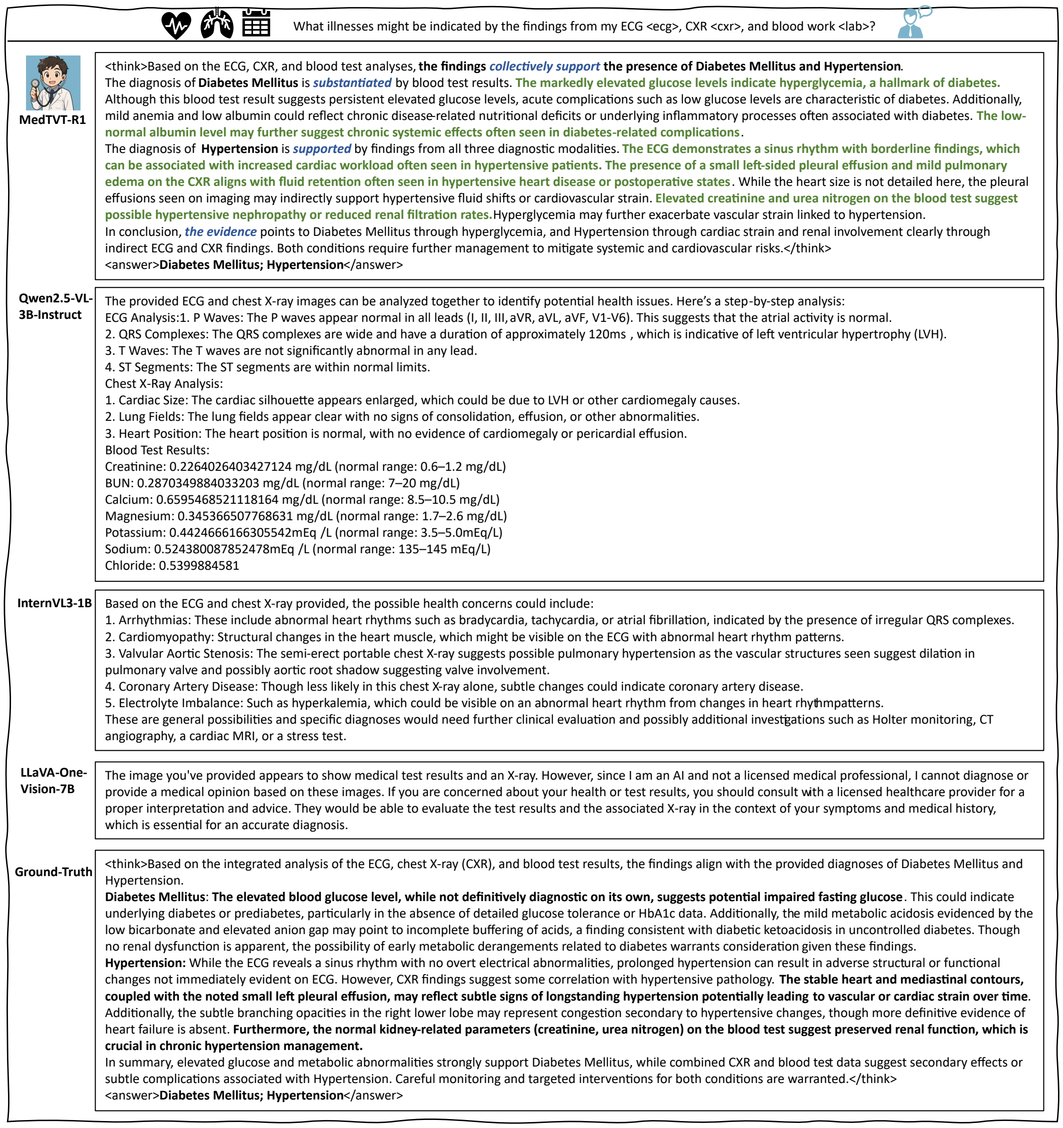

Figure 8: Performance of various MLLMs in handling medical reasoning and diagnosis. MedTVT-R1 approaches from the perspective of illness, tracing and identifying evidence of related diseases using the provided ECG, CXR, and LAB information. Qwen2.5-VL-3B-Instruct can analyze different modalities but lacks accuracy and cannot summarize diseases. InternVL3-1B combines modality information to determine disease types, though its accuracy is lacking. LLaVA-One-Vision-7B refuses to answer questions.

G The Use of LLMs

LLMs were utilized in this work for grammar checking and sentence refinement, aiming to enhance the clarity and readability of the text.